

TERAHERTZ RADIATION

https://doi.org/10.1070/QEL17453

Spectrally selective modulation of terahertz radiation beams

A.A. Ushakov, M. Matoba, N. Nemoto, N. Kanda, K. Konishi,
N.A. Panov, D.E. Shipilo, P.A. Chizhov, V.V. Bukin, M. Kuwata-Gonokami,
J. Yumoto, O.G. Kosareva, S.V. Garnov, A.B. Savel'ev

Abstract. **We report the results of an experimental study on the focusing of broadband terahertz (THz) radiation using lenses and Fresnel zone plates. The obtained data are compared with the results of numerical simulations. It is shown that the use of lenses for focusing THz radiation can lead to the appearance of a ring structure in the spatial distributions of its intensity. The use of Fresnel zone plates allows the spatial distribution of the THz radiation intensity to be varied at selected frequencies of the spectrum.**

Keywords: *terahertz radiation, diffraction, electro-optical detection, Fresnel zone plate.*

1. Introduction

Studies in the field of profiling terahertz (THz) radiation beams [1, 2] provide information about the physical processes that occur during the generation and propagation of electromagnetic radiation. In addition, the need to measure the beam intensity profile arises in connection with the study of nonlinear THz effects, for example, using the *z*-scanning technique [3]. Profiling of THz beams, primarily for laser-plasma sources, was performed using both electro-optical detection [4] and a matrix THz camera [5]. Later, spectrally selective profiling of THz beams was demonstrated, in which the THz radiation intensity profiles at individual frequency components were displayed using a set of bandpass filters [6]. Nevertheless, the problem of optimal conditions for focusing the pump radiation of two-frequency laser radiation into gaseous media remains not fully resolved from the viewpoint of the THz radiation directivity [4, 7, 8]. In addition, quite a large number of studies have been conducted recently on controlling the spatial distribution of THz radiation [9–12]. One of the possible methods of spectrally selective control of the spatial distribution of its intensity is the use of Fresnel zone plates [9, 13, 14].

A.A. Ushakov, V.V. Bukin, S.V. Garnov Prokhorov General Physics Institute of the Russian Academy of Sciences, ul. Vavilova 38, 119991 Moscow, Russia, e-mail: ushakov.aleksandr@physics.msu.ru;
M. Matoba, N. Nemoto, M. Kuwata-Gonokami Department of Physics, The University of Tokyo, 7 Chome-3-1 Hongo, Bunkyo City, Tokyo, Japan, 113-8654;
N. Kanda RIKEN Center for Advanced Photonics, RIKEN, 2-1 Hirosawa, Wako, Saitama, Tokyo, Japan 351-0198; Photon Science Centre, The University of Tokyo, 7 Chome-3-1 Hongo, Bunkyo City, Tokyo, Japan, 113-8654;
K. Konishi Institute for Photon Science and Technology, The University of Tokyo, 7 Chome-3-1 Hongo, Bunkyo City, Tokyo, Japan, 113-8654;
N.A. Panov, D.E. Shipilo, O.G. Kosareva, A.B. Saveliev Faculty of Physics and International Laser Centre, Lomonosov Moscow State University, Vorob'evy gory 1, 119991 Moscow, Russia; Lebedev Physical Institute, Russian Academy of Sciences, Leninsky prosp. 53, 119991 Moscow, Russia;
P.A. Chizhov Prokhorov General Physics Institute of the Russian Academy of Sciences, ul. Vavilova 38, 119991 Moscow, Russia; All-Russian Institute of Scientific and Technical Information, Russian Academy of Sciences, ul. Usievicha 20, 125190 Moscow, Russia;
J. Yumoto Department of Physics, The University of Tokyo, 7 Chome-3-1 Hongo, Bunkyo City, Tokyo, Japan, 113-8654; Institute for Photon Science and Technology, The University of Tokyo, 7 Chome-3-1 Hongo, Bunkyo City, Tokyo, Japan, 113-8654

Received 16 September 2020
Kvantovaya Elektronika **50** (11) 1029–1033 (2020)
Translated by M.A. Monastyrskiy

2. Experiments on measuring the THz beam profile

2.1. Measuring the THz radiation intensity profiles by a terahertz camera

In this work, profiling of a THz radiation beam was performed by recording two-dimensional distributions of its intensity in various planes using a THz camera [15]. The experimental setup is shown in Fig. 1.

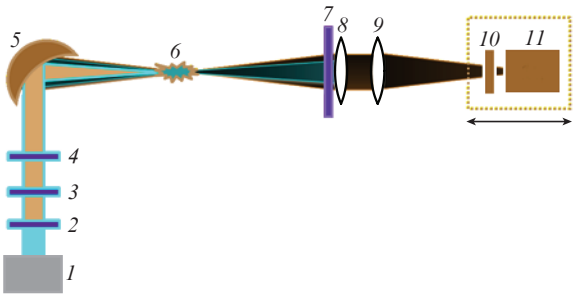

Figure 1. Scheme of the experimental setup for profiling THz beams: (*1*) femtosecond laser; (*2*) BBO crystal; (*3*) compensator plate; (*4*) phase plate; (*5*) parabolic mirror with $f = 190$ mm; (*6*) plasma; (*7*) polytetrafluoroethylene (PTFE) screen; (*8*) lens of Tsurupica material with $f = 5$ or 10 cm; (*9*) lens of Tsurupica material with $f = 10$ cm; (*10*) bandpass THz filter; (*11*) THz camera.

For laser plasma generation, radiation from a Ti:sapphire laser (centre wavelength of 800 nm, pulse duration of 35 fs, pulse energy of 2.7 mJ, and pulse repetition rate of 1 kHz) was used, which was passed through a nonlinear BBO crystal (the first-type phase-matching, 400-μm-thick crystal, 13% conversion efficiency), where it was partially converted to the second

harmonic. The radiation was then focused in the air by an off-axis parabolic mirror with a focal length f = 190 mm. For efficient generation of THz radiation, the radiation from a Ti:sapphire laser was transmitted to a parabolic mirror through a plate of the group velocity dispersion compensator and a phase plate (half-wave for the first harmonic and full-wave for the second). Thus, a two-colour radiation pulse was formed at the fundamental wave and at the second harmonic of laser radiation, and the pulses at both frequencies coincided in time and in the polarisation direction in the region of the beam waist. Then, THz radiation from a plasma source was focused using two biconvex lenses made of Tsurupica material (a refractive index of 1.52 in the optical and THz spectral ranges) with focal lengths of 10 or 5 cm (lens *8*) and 10 cm (lens *9*). The THz camera matrix (an array of 320 × 240 microbolometers, a pixel size of 23.5 × 23.5 μm [15]) was located in the close proximity to the THz beam waist. To prevent optical radiation from entering the matrix, a polytetrafluoroethylene (PTFE) screen was placed in front of lens *8*, which transmitted THz radiation and scattered optical radiation. In various planes perpendicular to the beam axis, in the vicinity of its waist, the THz radiation intensity distributions were measured with a step of 1 mm. To measure the spatial intensity distributions in individual bands of the THz spectrum, bandpass filters were installed in front of the camera aperture (centre transmission frequencies of 0.6, 0.8, 1.0, 1.3, 1.6, and 1.9 THz, a bandwidth of ~0.1 THz, transmission spectra are presented in [16]).

2.2. Measuring spatial distributions of THz radiation fields by an electro-optical technique

The setup for studying the spectrally selective focusing of THz radiation is schematically shown in Fig.2. The source of optical pumping was a Ti:sapphire laser system (pulse duration of 40 fs, pulse energy of 2.7 mJ, pulse repetition rate of 1 kHz, beam diameter of 12 mm at the $1/e^2$ level). The measurement of the spatial distribution of the electric field intensity of a THz pulse is based on the linear electro-optical effect. In the experiment, the depolarisation of pulsed probing optical radiation transmitted through a ZnTe crystal was measured. Depolarisation occurred due to the Pockels effect in the presence of a quasi-constant (within the femtosecond pulse duration) electric field of THz radiation. The laser radiation was divided into two parts: the first (main) part was used to generate THz radiation pulses in the source. To obtain a sufficiently high peak power of this radiation, we used a source based on optical rectification of femtosecond radiation pulses with a tilted intensity front in a lithium niobate crystal [17]. The second part, probing radiation constituting ~1% of the total radiation energy, passed through a variable delay line, and then through a polariser, a magnifying telescope and a quarter-wave plate. The elliptically polarised radiation beam was then combined with a THz beam at the beam splitter. The combined beams were directed into an electro-optical ZnTe crystal (size of 10 × 10 × 0.5 mm, ⟨110⟩ cut). The crystal surface was mapped by a telescope onto a digital camera matrix (Basler acA2040-25gm-NIR, 2048x2048 pixels). An optical polariser was positioned in front of the matrix to transmit vertically polarised radiation.

During the experiments, images of the crystal were recorded in the presence of THz fields, $I_{\text{sign}}(x,y,\tau)$, and, in their absence, $I_{\text{ref}}(x,y,\tau)$. This recording was performed at various delays between THz and probe pulses. The relationship between the electric field intensity distribution of a THz pulse and the measured intensity distributions is given by the following expression [13, 18, 19]:

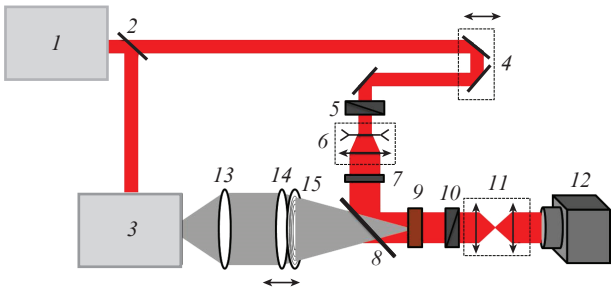

Figure 2. Scheme of the experimental setup:
(*1*) femtosecond laser; (*2*) beam splitter; (*3*) THz radiation source on a lithium niobate crystal; (*4*) variable delay line; (*5*) polariser; (*6*) telescope; (*7*) quarter-wave plate; (*8*) film beam splitter; (*9*) ZnTe crystal; (*10*) polariser; (*11*) telescope; (*12*) CMOS camera; (*13*) PTFE lens (f = 6 cm); (*14*) PTFE lens (f = 15 cm); (*15*) zone plate.

$$E_{\text{THz}}(x,y,\tau) \propto \frac{I_{\text{sign}}(x,y,\tau) - I_{\text{ref}}(x,y,\tau)}{I_{\text{ref}}(x,y,\tau)}. \qquad (1)$$

Processing of the obtained images made it possible to measure the spatiotemporal dependence of the electric field strength $E_{\text{THz}}(x,y,\tau)$. As a result, we obtained a three-dimensional array of E_{THz} values with a size of 250 × 2048 × 2048 points in the region of 50 × 10 × 10 ps mm mm. Then, a discrete Fourier transform was applied to this array along the time coordinate, resulting in spatial distributions of the spectral components of THz radiation. The thus obtained distributions had a spectral width of 5 THz, while the frequency shift between them was 20 GHz.

The THz radiation pulse under study was formed as follows: the radiation from the lithium niobate generator was collimated by lens *13* with f = 6 cm. The beam was then focused by lens *14* with f = 15 cm. To provide spatially spectral modulation of radiation, various Fresnel plates were placed behind lens *14*, made by gluing aluminium foil rings onto a polyimide film. The radii of the rings in the zone plates were chosen based on the expression [20]

$$r_n = \sqrt{(n+1)\lambda z}\,, \qquad (2)$$

where r_n is the radius of the nth Fresnel zone; and z is the focal length for radiation at the wavelength λ. In our case, we used two zone plates with focal lengths of 20 cm for radiation at frequencies of 600 and 800 GHz (λz = 100 and 75 mm^2, respectively). Photographs of these plates are shown in Fig. 3. The location of the zone plate directly behind lens *14* led to a reduction in the focal length of the optical system under consideration to 8.6 cm for radiation at the corresponding frequency.

3. Results of experiments

In the experiment described in Section 2.1, the THz radiation intensity distributions were measured, some of which are shown in Fig. 4. To demonstrate the features of the intensity distributions of THz radiation revealed in the course of its focusing, numerical simulation was performed in the frame-

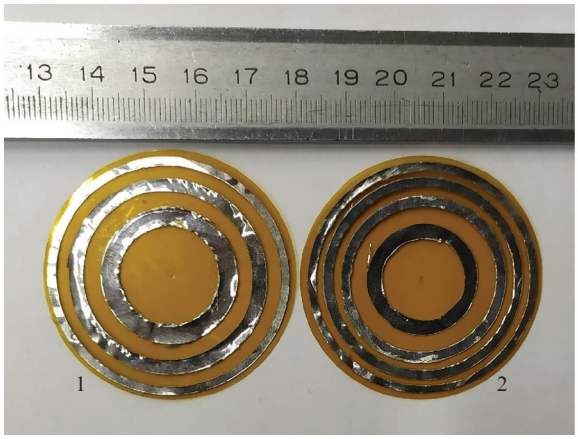

Figure 3. Zone plates with a focal length of 20 cm for radiation at frequencies of (1) 600 and (2) 800 GHz.

work of the propagation equation in the paraxial approximation, which was solved in Fourier space:

$$\frac{\partial \hat{E}(k_x,k_y,z)}{\partial z} = \mathrm{i}\frac{k_x^2+k_y^2}{2c\omega_0}\hat{E}(k_x,k_y,z), \qquad (3)$$

where $\hat{E}(k_x,k_y,z)$ is the two-dimensional Fourier transform of the fields $E(x,y,z)$; ω_0 is the original frequency of THz radiation; and c is the speed of light. For calculations, a Gaussian beam with a radius of 100 μm was chosen as a source (this value is comparable to the transverse size of the plasma channel itself and the radiation wavelength). The original beam propagated from the geometric focus of lens *8* (see Fig. 1). Then, when passing through both lenses, a parabolic phase incursion equivalent to the action of each of the lenses was added to the source radiation, and the beam was limited by the lens aperture. After that, THz radiation intensity profiles were constructed at selected frequencies in the focal plane of lens *9*, as well as in front and behind the focal plane at a distance of 1.5 cm from it. The distributions shown in Fig. 4 are averaged over the frequency ω_0, with weights corresponding to the experimental spectra. To simulate the zone plate, the radiation transmitted through lens *9* was modulated in amplitude in accordance with the calculated radii of the Fresnel zones.

The numerical aperture of the optical elements in the experiment was quite large, reaching 0.3–0.5. Nevertheless, the paraxial approximation can be used to simulate our problem, which was demonstrated earlier [21]. For this reason, the propagation equations (3) were chosen for calculating the spatial spectrum of THz radiation. The THz radiation intensity profiles in the planes in which the measurements were performed are shown in Fig. 4. From the results of both experiments and numerical simulation, it follows that there are differences in intensity profiles in the planes located at equal distances from the focusing lens waist (in front and behind it). Despite the fact that the main part of THz radiation falls into the aperture of lens *8* (which follows from the data on the directional patterns of this radiation in the far zone [16]) and at the same time has a unimodal structure with a maximum on the axis, the rings are still visible in radiation propagation, which is a manifestation of its diffraction at the lens aperture. This conclusion is confirmed by the fact that the profile structure changes depending on the lenses used for imaging. Another possible cause of the rings may be spherical aberrations in the lenses, which were not considered in the simulation.

In the experiment with zone plates described in Section 2.2, two-dimensional distributions of the electric field intensity of THz pulses were measured, shown in Fig. 5.

When use is made of only lens *14* in the plane $z = 15$ cm, a pronounced maximum is observed for radiation at all frequencies, and with a decrease in the radiation wavelength, the beam size decreases, which is consistent with the classical formula from the diffraction theory [20]:

$$\rho = \frac{\lambda f}{\pi d}, \qquad (4)$$

where ρ is the beam radius at the waist; and d is the beam diameter. In the plane $z = 8.6$ cm, in the absence of zone plates, the beam diameter increases, while the field amplitude decreases. The installation of the zone plate leads to a shift in the focal plane for THz radiation at the selected frequency,

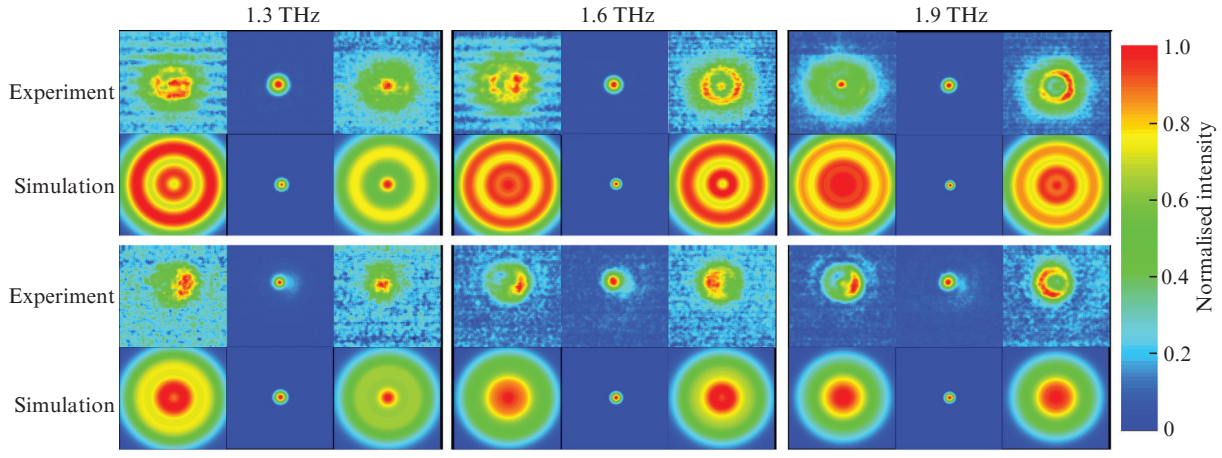

Figure 4. Experimentally measured and numerically calculated THz radiation intensity profiles for frequencies of 1.3, 1.6, and 1.9 THz in the focal plane of lens 9 (Fig. 1) and in planes located at a distance of 1.5 cm from the focal plane (in front and behind). The upper row of profiles was obtained at $f = 10$ and 10 cm, the lower one, at $f = 5$ and 10 cm, respectively.

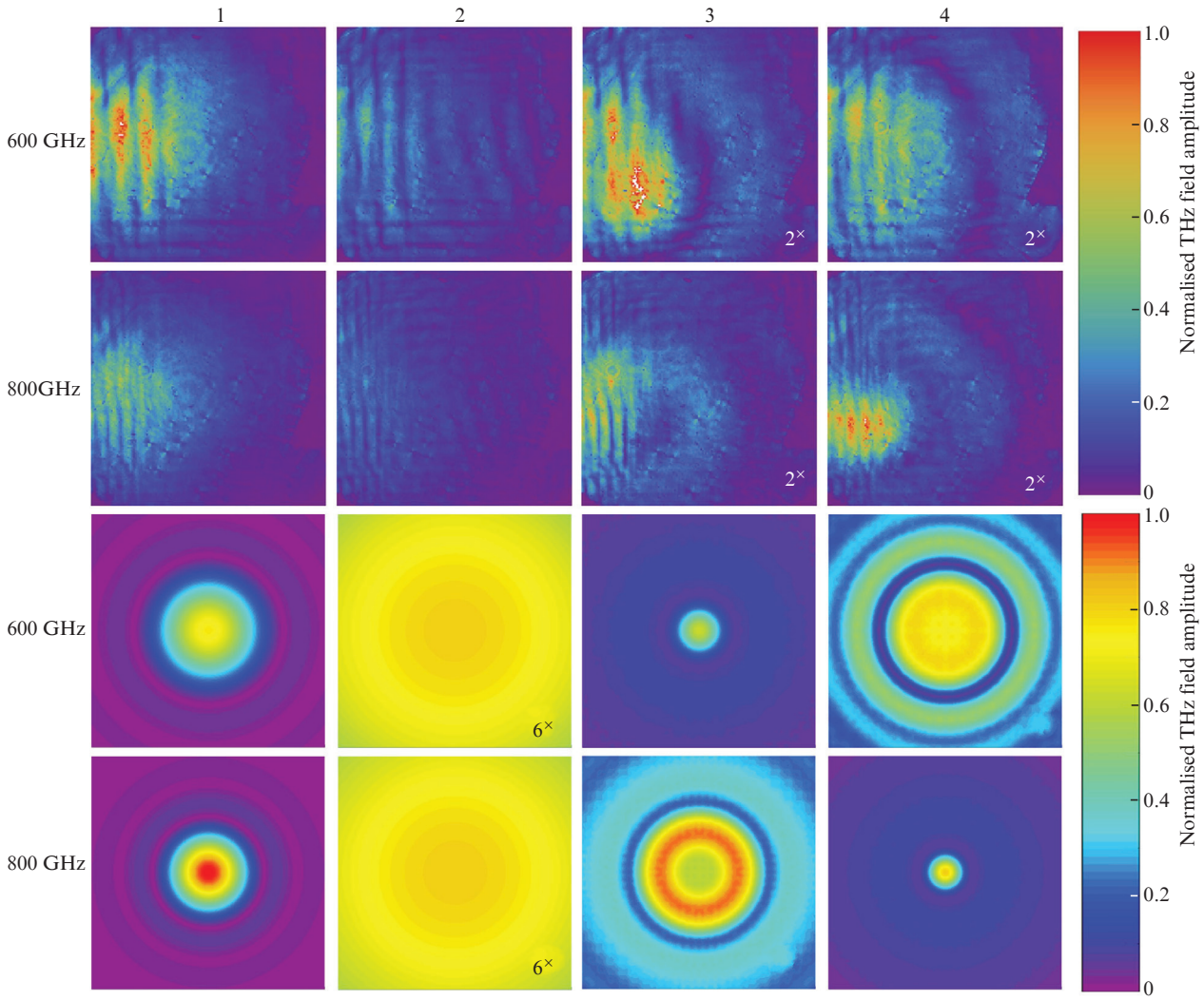

Figure 5. Experimentally obtained (top) and numerically calculated (bottom) distributions (10 × 10 mm) of THz radiation fields at frequencies of 600 and 800 GHz in planes x, y at (1) z = 15 cm (focal plane of lens *14* without using zone plates); (2) z = 8.6 cm (focal plane of the system consisting of lens *14* and a zone plate) in the case of using only lens *14* (diverging THz beam); (3) z = 8.6 cm in the case of using lens *14* and a zone plate with f = 20 cm for radiation at a frequency of 600 GHz; (4) z = 8.6 cm in the case of using lens *14* and a zone plate with f = 20 cm for radiation at a frequency of 800 GHz.

which can be observed in distributions 3 and 4 (Fig. 5). In this case, it can be seen that for radiation with a frequency other than the frequency corresponding to the zone plate with f = 20 cm, a pronounced maximum does not occur, which allows spectral control of the focusing of THz radiation. It is also seen that the total amplitude of the radiation field at the selected frequency decreases but remains comparable to the amplitude in the case of conventional focusing of radiation with a lens. The obtained distributions show that the beam diameter in the experiment differs slightly from the calculated one, which leads to differences between the experimental results and the numerical simulation data. These differences can also be explained by diffraction distortions due to imperfect alignment of the optical system. Nevertheless, the spatial distributions 3 and 4 in Fig. 5 clearly demonstrate a qualitative agreement between the experimental and numerical results. However, the experimentally obtained distributions contain vertical bands that do not change their position and structure when the configuration of optical elements changes, which may be due to the properties of the THz radiation source or the imperfect alignment of the experimental setup.

4. Conclusions

We have performed experimental and numerical studies of the spatial distributions of the field amplitudes and intensities of THz radiation focused by zone plates and lenses. It is shown that the use of zone plates makes it possible to control the radiation divergence at selected frequencies. Profiling of focused THz beams from a laser-plasma source revealed an inhomogeneity in the spatial structure of the THz radiation intensity distributions, which is a consequence of diffraction effects. This fact may become fundamental in z-scanning experiments to study the nonlinear interaction of THz radiation with matter.

Acknowledgements. This work was supported by the Presidium of the Russian Academy of Sciences (Programme No. 6 'New approaches to the creation and study of extreme states of matter'), Presidential scholarships for young scientists and postgraduate students (SP-500.2019.4, SP-2453.2018.2), Russian Foundation For Basic Research (Grant No. 18-52-16020), and the 'Photon Advanced Network' Programme of

the Ministry of Education, Culture, Sports, Science, and Technology (MEXT).

References

1. Klarskov P., Strikwerda A.C., Iwaszczuk K., Jepsen P.U. *New J. Phys*., **15**, 075012 (2013).
2. Klarskov P., Strikwerda A.C., Wang T., Zalkovskij M., Jepsen P.U. *Proc. SPIE*, **8624**, 86240D (2013).
3. Chai X., Ropagnol X., Ovchinnikov A., Chefonov O., Ushakov A., Garcia-Rosas C.M., Isgandarov E., Agranat M., Ozaki T., Savel'ev A. *Opt. Lett*., **43**, 5463 (2018).
4. Zhong H., Karpowicz N., Zhang X.-C. *Appl. Phys. Lett*., **88**, 261103 (2006).
5. Klarskov P., Strikwerda A.C., Iwaszczuk K., Jepsen P.U. *New J. Phys*., **15**, 075012 (2013).
6. Klarskov P., Zalkovskij M., Strikwerda A.C., Jepsen P.U. *Proc. CLEO: 2014*, 6–7 (2014).
7. Ushakov A.A., Panov N.A., Chizhov P.A., Shipilo D.E., Bukin V.V., Savel'ev A.B., Garnov S.V., Kosareva O.G. *Appl. Phys. Lett*., **114**, 081102 (2019).
8. Ushakov A.A., Matoba M., Nemoto N., Kanda N., Konishi K., Chizhov P.A., Panov N.A., Shipilo D.E., Bukin V.V., Kuwata-Gonokami M., Yumoto J., Kosareva O.G., Garnov S.V., Savel'ev A.B. *JETP Lett*., **106**, 706 (2017).
9. Wang X., Xie Z., Sun W., Feng S., Cui Y., Ye. J., Zhang Y. *Opt. Lett*., **38**, 4731 (2013).
10. Shang Y., Wang X., Sun W., Han P., Ye. J., Feng S., Zhang Y. *Opt. Express*, **27**, 14725 (2019).
11. Kulya M., Semenova V., Gorodetsky A., Bespalov V.G., Petrov N.V. *Appl. Opt*., **58**, 1 (2018).
12. Siemion A. *J. Infr., Millimet., Terahertz Waves*, **40**, 477 (2019).
13. Ushakov A.A., Chizhov P.A., Bukin V.V., Garnov S.V. *Bull. Lebedev Phys. Inst*., **46,** 336 (2019) [*Kr. Soobshch. Fiz. FIAN*, **11**, 8 (2019)].
14. Wiltse J. C. *Proc. SPIE*, **5411**, 127 (2004).
15. Nemoto N., Kanda N., Imai R., Konishi K., Miyoshi M., Kurashina S., Sasaki T., Oda N., Kuwata-Gonokami M. *IEEE Trans. Microw. Theory Techn*., **6**, 175 (2016).
16. Ushakov A.A., Chizhov P.A., Andreeva V.A., Panov N.A., Shipilo D.E., Matoba M., Nemoto N., Kanda N., Konishi K., Bukin V.V., Kuwata-Gonokami M., Kosareva O.G., Garnov S.V., Savel'ev A.B. *Opt. Expres*s, **26**, 18202 (2018).
17. Hebling J., Yeh K.-L., Hoffmann M.C., Bartal B., Nelson K.A. *J. Opt. Soc. Am. B*, **25**, B6 (2008).
18. Ushakov A.A., Chizhov P.A., Bukin V.V., Savel'ev A.B., Garnov S.V. *J. Opt. Soc. Am. B*, **35**, 1159 (2018).
19. Ushakov A.A., Chizhov P.A., Bukin V.V., Garnov S.V., Savel'ev A.B. *Quantum Electron*., **48**, 487 (2018) [*Kvantovaya Elektron*., **48**, 487 (2018)].
20. Akhmanov S.A., Nikitin S.Yu. *Physical Optics* (Oxford: Clarendon Press, 1997; Moscow: Nauka, 1991).
21. Fedorov V.Y., Chanal M., Grojo D., Tzortzakis S. *Phys. Rev. Lett*., **117**, 043902 (2016).